The Multiple-Point Variogram of Images for Robust Texture Classification

Tuan D. Pham
Department of Biomedical Engineering
Linkoping University
Linkoping 58183, Sweden

***Abstract*—Most texture analysis techniques require training data to perform classification or retrieval of images. In many practical situations, the amount of data representing different texture classes can be too limited to satisfy the training of a reliable classifier. Therefore, finding an effective feature of texture is very useful to cope with a variety of applications. This paper presents the extension of the two-point variogram to multiple-point variogram of images for texture feature extraction, which is also robust to noise and computationally economic. The matching of the variogram functions for pattern classification can be enhanced with the use of a spectral distortion measure without the requirement of training data. Experimental results and comparison with other methods, which require training data, suggest the usefulness of the proposed approach.**

***Keywords*—Texture analysis, Variograms, Distortion measures.**

I. Introduction

The concept of texture is still not well-defined, the aim of texture analysis is therefore to acquire some rigorous mathematical formulations that can distinguish different classes of texture in images. This difficulty makes texture analysis an on-going challenging problem in image classification and retrieval. A large number of techniques have been developed for texture analysis, where a collection of important developments in this field were reviewed in [1]. Recent developments and applications of texture analysis and classification can be found in [2]-[8].

In general, methods for texture analysis consist of two main domains: structural and statistical [9]. While the structural approach analyzes an image in terms of a transform to expose the detail of its structure, the statistical approach examines the statistics of the properties of an image. This study explores a spatial statistical methodology for extracting effective texture feature of an image based on the notion of the variogram of an image. In fact, the use of the variograms, which form the fundamental concept of geostatistics [10], has been proposed for texture analysis over the years [11]-[17]. The departure of the present study from other variogram-based methods is that it introduces the formulation of the multiple-point variogram of an image, while other methods apply the two-point variogram to capture the spatial relationship of pixels in an image. Advantages of the multiple-point variogram over the two-point variogram for image analysis are two-fold: better classification accuracy and faster computational speed. A logical basis for the adoption of the multiple-point variogram is that mathematical measures that are used to quantify the dissimilarity or distance between objects can be either a vector or a scalar. The distinct difference between these two classes can be appreciated by their definitions: scalars are quantities that are described by a magnitude, whereas vectors are those that are characterized by both a magnitude and a direction. The latter class conveys more information than the former. Furthermore, this study utilizes a physically reasonable and computationally tractable tool of spectral distortion measures to robustly measure the dissimilarity between two spectra of the variograms.

The rest of this paper is organized as follows. Section II presents the extension of the two-point variogram to the multiple-point variogram, which is well-suited for image analysis. Section III describes the matching of variograms using as spectral distortion measure known as the log-likelihood ratio distortion. Finally, experimental results and discussion are given in Section IV.

II. The Multiple-Point Variogram of Images

Let Z, x, and h be a random function, a spatial location, and a lag distance in the sampling space, respectively. The random function $Z(x)$ is assumed to be second-order stationary, which implies the mean m and variance σ^2 are location-independent: $m(x) = m$ and $\sigma^2(x) = \sigma^2$, for all locations x in the space. The variogram of the random function is defined as [10], [18]

$$2\gamma(h) = Var[Z(x) - Z(x+h)], \tag{1}$$

where $\gamma(h)$ is the semi-variogram of the random function. This definition of the variogram, $2\gamma(h)$, or semi-variogram, $\gamma(h)$, assumes that the random function changes within the space, but $\gamma(h)$ is independent of spatial location and depends only on the distance of the pair of the considered variates. To simplify technical jargon, the semi-variogram is now referred to as the variogram, unless mathematical expression requires a precise definition.

Based on Equation (1), the variogram is equivalent to

$$\gamma(h) = \frac{1}{2} E\left[\{Z(x) - Z(x+h)\}^2\right] \tag{2}$$

Let $Z(x_i)$, $i = 1, 2, \dots, n$, be a sampling of size n, the unbiased estimator for the variogram, which is called the experimental variogram, of the random function is expressed as

$$\gamma(h) = \frac{1}{2N(h)} \sum_{i=1}^{N(h)} [Z(x_i) - Z(x_i + h)]^2, \quad (3)$$

where $N(h)$ is the number of variable pairs separated by h.

The experimental variogram defined in Equation (3) is known as the two-point variogram in geostatistics (not to be confused with multiple-point geostatistics [19]). Taking the advantage of both spatial and sequential information of an image, the two-point variogram can be readily extended to the multiple-point variogram of an image as follows.

Let $Z(\mathbf{x}_i)$ be the either the pixel values of an image row i or column i, and $Z(\mathbf{x}_i + h)$ the pixel values of an image row $i+h$ or column $i+h$: $\mathbf{x}_i = (x_{i1}, x_{i2}, \ldots, x_{ip})$ or $\mathbf{x}_i = (x_{1i}, x_{2i}, \ldots, x_{pi})$, assuming that the image has equal numbers of rows and columns for simplified mathematical expression. The multiple-point variogram of an image can be defined as

$$\gamma(h) = \frac{1}{2M(h)} \sum_{i=1}^{M(h)} ||Z(\mathbf{x}_i) - Z(\mathbf{x}_i + h)||^2, \quad (4)$$

where $M(h)$ is the number of pairs of image rows and columns that are separated by distance h, and $||\cdot||$ is any inner product induced norm on $\mathcal{R}^p$ (the Euclidean norm is used in this study); moreover, the exponent of 2 can be omitted to simplify the expression, which is analogous to the use of the absolute value of the pixel difference for the variogram [11].

III. Variogram Matching with Log-Likelihood Ratio Distortion Measure

Given an experimental variance at lag h, $\gamma(h)$ can be approximated as a linear combination of the past p variances, such that

$$\tilde{\gamma}(h) = -\sum_{i=1}^{p} a_i \gamma(h-i) \quad (5)$$

where a_i, $i = 1, \ldots, p$ are the linear predictive coding (LPC) coefficients [20], assumed to be constant over the range of the variances, and to be optimally determined.

The error between $\tilde{\gamma}(h)$ and $\gamma(h)$ is

$$e(h) = \gamma(h) + \sum_{i=1}^{p} a_i \gamma(h-i) \quad (6)$$

By minimizing the sum of squared errors, the pole parameters $\{a_i\}$ of the LPC model can be determined as follows.

$$\mathbf{a} = -\mathbf{R}^{-1}\,\mathbf{r} \quad (7)$$

where $\mathbf{a}$ is a $p \times 1$ vector of the LPC coefficients, $\mathbf{R}$ is a $p \times p$ autocorrelation matrix, and $\mathbf{r}$ is a $p \times 1$ autocorrelation vector whose elements are defined as

$$r_i = \sum_{h=0}^{N} \gamma(h)\gamma(h+i),\ i = 1, \ldots, p. \quad (8)$$

TABLE I. Classification rates (%) of ten-texture image group obtained from two-point and multiple-point variograms.

	Two-point variogram		Multiple-point variogram	
Image ID	D_E	D_{LLR}	D_E	D_{LLR}
D4	100	100	97.22	100
D9	100	100	100	100
D19	61.11	73.61	61.11	69.44
D21	84.72	97.11	81.95	100
D24	77.78	98.61	91.67	100
D28	80.56	93.06	76.39	83.33
D29	34.72	44.11	52.78	69.44
D36	37.50	38.89	34.72	36.11
D37	86.11	86.11	90.28	93.06
D38	80.56	88.89	83.33	93.06

TABLE II. Comparison of classification rates (%) of ten-texture image group.

Filtering methods (with training)	52.6 (average), 67.7 (best)
Spectral histogram (with training)	83.1
Two-point variogram (D_{LLR}) (no training)	82.0
Multiple-point variogram (D_{LLR}) (no training)	84.4

Let $S(\omega)$ and $S'(\omega)$ be the spectral density functions of a p-th order all-pole model of the variograms $\gamma(h)$ and $\gamma'(h)$, respectively, where ω is normalized frequency ranging from -π to π. The spectral density $S(\omega)$ is defined as [20]

$$S(\omega) = \frac{\sigma^2}{|A|^2}, \quad (9)$$

where $\sigma^2 = \mathbf{a}^T\mathbf{R}\mathbf{a}$, and $A = 1 + a_1 e^{-i\omega} + \ldots + a_p e^{-ip\omega}$.

The log-likelihood-ratio (LLR) distortion measure between $S(\omega)$ and $S'(\omega)$, denoted as $D_{LLR}(S, S')$, is defined as [21]

$$D_{LLR}(S, S') = \log \frac{\mathbf{a}'^T\mathbf{R}\mathbf{a}'}{\mathbf{a}^T\mathbf{R}\mathbf{a}}, \quad (10)$$

where $\mathbf{a}'$ is the vector of the LPC coefficients of S'.

IV. Results and Discussion

The images used in this experiment are of the well-known Brodatz database [22]. The size of the original images is 640×640 pixels, which are obtained from [23]. The test

TABLE III. Classification rates (%) of two-texture image groups.

	Figure (a)	Figure (b)	Figure (c)
Two-point variogram	100	100	100
Multiple-point variogram	100	100	100

TABLE IV. Classification rates (%) of six-texture image group obtained from two-point and multiple-point variograms using D_{LLR}.

Image ID	Two-point variogram	Multiple-point variogram
D4	75.00	80.56
D5	100	100
D12	100	100
D17	100	100
D84	100	100
D92	98.61	97.22
Average	95.60	96.30

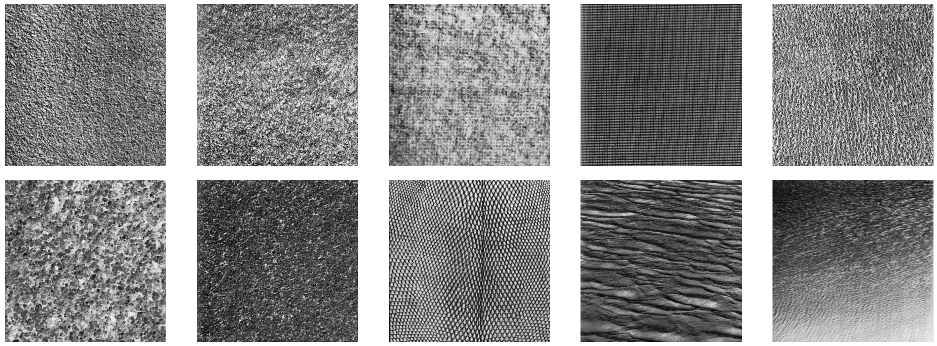

Fig. 1. Ten-texture 640 × 640 Brodatz image image group, from left to right: 1st row: D4, D9, D19, D21, and D24; 2nd row: D28, D29, D36, D37, and D38.

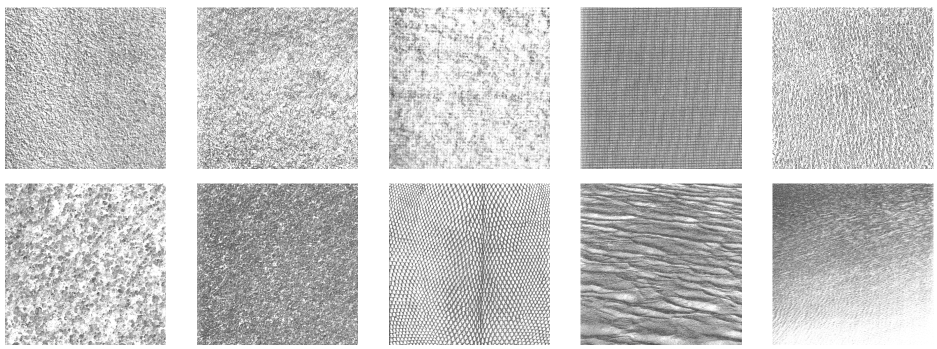

Fig. 2. Ten-texture 640 × 640 Brodatz image image group, degraded with white Gaussian noise of 0.01 variance and 0.3 mean, from left to right: 1st row: D4, D9, D19, D21, and D24; 2nd row: D28, D29, D36, D37, and D38.

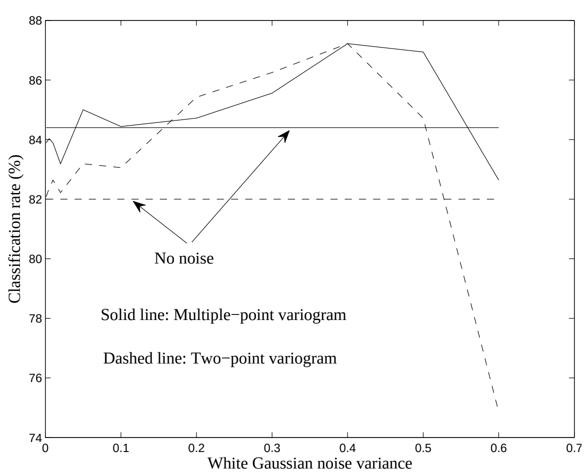

Fig. 3. Classification rates of ten-texture image group versus white Gaussian noise variance of 0.01 and variable mean.

images are divided into two sets, which are after [24]: 10-texture and 2-texture image groups. The 10-texture group includes D4, D9, D19, D21, D24, D28, D29, D36, D37, and D38. The 2-texture groups consist of D4 and D84, D12 and D17, and D5 and D92. Figure 1 and Figure 4 show the images of the 10-texture and 2-texture groups, respectively. To test the performance of the proposed method without the need for training data, the experiment was set up using the same procedure as described in [25]. Each original image was divided into 9 non-overlapping sub-images (except 5 columns and 5 rows of pixels for the corresponding sub-images in the last row-wise and column-wise partitions), yielding each sub-image of size 215×215 pixels. Thus, a perfect classification (100%) for each test sub-image is the successful search of 8 closest matches.

For the 10-texture image group, the classification rate obtained from the two-point variogram using the Euclidean norm and LLR distortion measure are 74.31% and 82.08%, respectively; and the multiple-point variogram resulted in 76.95% using the Euclidean norm, and 84.44% using the LLR distortion measure. These results show that the multiple-point variogram performs better than the two-point variogram, and both cases suggest the preference of the LLR over the Euclidean norm. Table I shows the individual classification rates obtained from the two-point and multiple-point variograms using the Euclidean norm and LLR distortion measures, in which D29 was largely better classified by the multiple-point variogram. The comparison of the results obtained from the variograms and the filtering [24] and spectral-histogram methods [26], which requires training data, are shown in Table II. These comparative results demonstrates the high performance

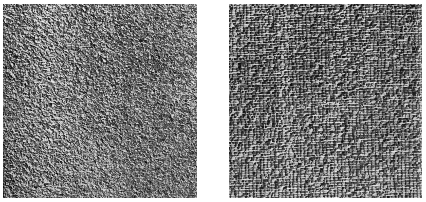

(a)

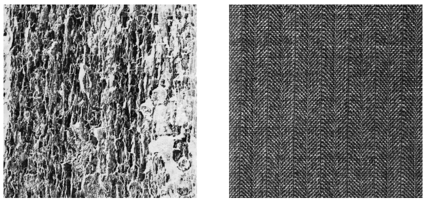

(b)

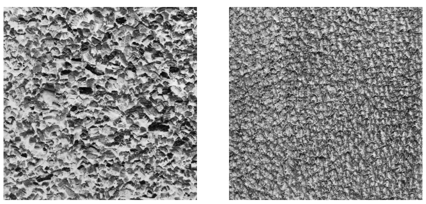

(c)

Fig. 4. Two-texture 640×640 Brodatz image groups, from left to right: (a): D4 and D84, (b): D12 and D17, (c): D5 and D92.

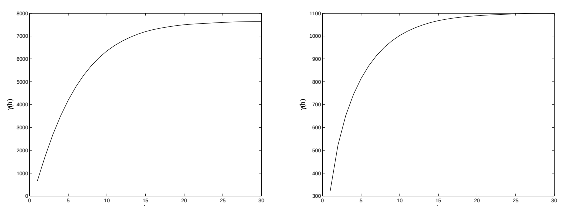

(a)

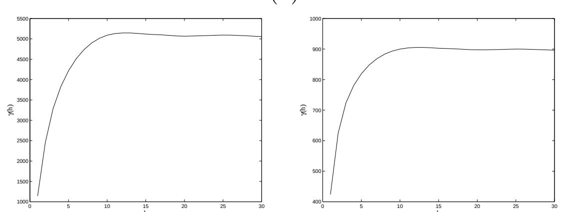

(b)

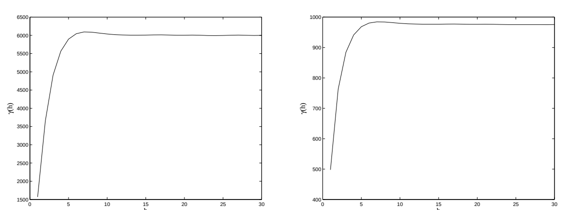

(c)

Fig. 5. Variograms of D5 (a), D92 (b), and D4 (c) where the left and right figures are two-point and multiple-point variograms, respectively.

of the multiple-point variogram for texture classification. To test the robustness of the proposed approach with the use of the LLR, the images were degraded with white Gaussian noise with variance of 0.01 and variable means: 0.001, 0.005, 0.01, 0.02, 0.05, 0.1, 0.2, 0.3, 0.4, 0.5, and 0.6. It is interestingly observed that adding noise to the texture, the classification rates using either the two-point or multiple-point variograms were stable or even improved up to the noise mean of 0.6, where the highest improvement (87.22%) for both variograms is at the noise mean of 0.4. Figure 2 shows the ten-texture image group degraded with mean of 0.3 and variance of 0.01. Figure 3 plots the classification rates obtained from the two-point or multiple-point variograms versus the noise levels. Due to the stochastic nature of the texture, the addition of noise at some certain levels to the images allows the variograms to better distinguish different types of similar textures. Figure 3 shows the classification by the two-point variogram that failed sharply at the noise variance of 0.6 (82.08% vs. 74.86%), but slightly for the multiple-point variogram (84.44% vs. 82.64%).

Figure 5 presents the plots of the two-point and multiple-point variograms of D5 and D92, as shown in Figure 4(c). It has been pointed out that the classification of this pair of images was very difficult for many texture analysis techniques [24]. Both variograms of this pair of images can discriminate the difference between these two textures, and with the use of the LLR distortion measure, a perfect classification was achieved. Table III lists the classification rates of the two-texture image groups, in which both variograms achieved the perfect results (zero classification errors) for the three pairs of images. As discussed in [24], the minimum classification errors obtained among 9 texture feature extractors, using learning vector quantization (requiring training data), were 1.9 (co-occurrence) for Figure 4(a), 0.6 (Daubechies) for Figure 4(b), and 2.5 (discrete cosine transform) for Figure 4(c).

Furthermore, Table IV shows the classification rates of the six images shown in Figure 4, where most classication rates are maximum, except for D4 (75% for two-point variogram, and 80.56% for multiple-point variogram), and D92 (98.61% for two-point variogram, and 97.22% for multiple-point variogram) The plots of the two-point and multiple-point variograms of D4, which presented in Figure 4(a), are shown in Figure 5. Although the classification rate for D92 obtained from the multiple-point variogram is lower than the two-point variogram, its total classification average (96.30%) is higher than the two-point variogram (95.60%). Once again, these results demonstrate that the high performance of the multiple-point variogram.

For an image of 256×256 pixels, the time taken for executing the Matlab code on a computer ProBook 6570b, Core i7, Windows 8, to calculate 30 lags for the two-point variogram was 0.12 seconds, and multiple-point variogram was 0.04 seconds. This timing shows the multiple-point variogram is 3 times faster than the two-point variogram for such an image size. For an image of size 640×640 pixels, the computational times required for the two-point and multiple-point variograms were 1.02 and 0.27 seconds, respectively; which shows the multiple-point variogram is approximately 4 times faster than the two-point variogram.

References

[1] M. Mirmehdi, X. Xie, J. Suri, *Handbook of Texture Analysis*. London: Imperial College Press, 2008.

[2] Y. Dong, D. Tao, X. Li, J. Ma, J. Pu, "Texture classification and retrieval using shearlets and linear regression", *IEEE Trans Cybernetics*, vol. 45, pp. 358-369, 2015.

[3] Y. Song, W. Cai, Q. Li, F. Zhang, D.D. Feng, H. Huang, "Fusing subcategory probabilities for texture classification", *Proc. IEEE Conf. Computer Vision and Pattern Recognition* pp. 4409-4417, 2015.

[4] Z. Zhu, X. You, C.L. P. Chen, D. Tao, W. Ou, X. Jiang, J. Zou, "An adaptive hybrid pattern for noise-robust texture analysis", *Pattern Recognition*, vol. 48, pp. 2592-2608, 2015.

[5] A. Hafiane, K. Palaniappan, G. Seetharaman, "Joint adaptive median binary patterns for texture classification", *Pattern Recognition*, vol. 48, pp. 2609-2620, 2015.

[6] T. Song, H. Li, F. Meng, Q. Wu, B. Luo, "Exploring space-frequency co-occurrences via local quantized patterns for texture representation", *Pattern Recognition*, vol. 48, pp. 2621-2632, 2015.

[7] S. Hegenbart, A. Uhl, "A scale- and orientation-adaptive extension of local binary patterns for texture classification", *Pattern Recognition*, vol. 48, pp. 2633-2644, 2015.

[8] S. Wang, Q. Wu, X. He, J. Yang, Y. Wang "Local n-ary pattern and its extension for texture classification", *IEEE Transactions on Circuits and Systems for Video Technology*, vol.25, 2015. DOI: 10.1109/TCSVT.2015.2406198. Publication in a future issue, but not fully edited.

[9] M.S. Nixon, A.S. Aguado, *Feature Extraction & Image Processing for Computer Vision*, 3rd Edition. Oxford: Academic Press, 2012.

[10] R.A. Olea, *Geostatistics for Engineers and Earth Scientists.* Boston: Kluwer Academic Publishers, 1999.

[11] J.R. Carr, F.P. de Miranda, "The semivariogram in comparison to the co-occurrence matrix for classification of image texture", *IEEE Trans. Geoscience and Remote Sensing*, vol. 36, pp. 1945-1952, 1998.

[12] A. Jakomulska, K.C. Clarke, "Variogram-derived measures of textural image classification", *Quantitative Geology and Geostatistics*, vol. 11, pp. 345-355, 2001.

[13] P. Li, T. Cheng, J. Guo, "Multivariate image texture by multivariate variogram for multispectral image classification", *Photogrammetric Engineering and Remote Sensing*, vol. 75, pp. 147-157, 2009.

[14] A. Balaguer-Beser, T. Hermosilla, J. Recio, L.A. Ruiz, "Semivariogram calculation optimization for object-oriented image classification", *Modelling in Science Education and Learning*, vol. 4, pp. 91-104, 2011.

[15] T.D. Pham, "Geostatistical entropy for texture analysis: an indicator kriging approach", *Int. J. Intelligent Systems*, vol. 29, pp. 253-265, 2014.

[16] T.D. Pham, D.T.P. Le, J. Xu, D.T. Nguyen, R.G. Martindale, C.W. Deveney, "Personalized identification of abdominal wall hernia meshes on computed tomography", *Computer Methods and Programs in Biomedicine*, vol. 113,) pp. 153-161, 2014.

[17] T. Tsunoyama, T.D. Pham, T. Fujita, T. Sakamoto, "Identification of intestinal wall abnormalities and ischemia by modeling spatial uncertainty in computed tomography imaging findings", *Computer Methods and Programs in Biomedicine*, vol. 117, pp. 30-39, 2014.

[18] E. Gringarten, C.V. Deutsch, "Teacher's aide variogram interpretation and modeling", *Mathematical Geology*, vol. 33, pp. 507-534, 2001.

[19] E. Meerschman, G. Pirot, G. Mariethoz, J. Straubhaar, M.V. Meirvenne, P. Renard, "A practical guide to performing multiple-point statistical simulations with the Direct Sampling algorithm", *Computers & Geosciences*, vol. 52, pp. 307-324, 2013.

[20] L. Rabiner, B.H. Juang, *Fundamentals of Speech Recognition*. New Jersey: Prentice Hall, 1993.

[21] N. Nocerino, F. Soong, L. Rabiner, D. Klatt, "Comparative study of several distortion measures for speech recognition", *Proc. IEEE Int. Conf. Acoustics, Speech, and Signal Processing*, vol. 10, pp. 25-28, 1985.

[22] P. Brodatz, *Textures: A Photographic Album for Artists and Designers*. New York: Dover, 1966.

[23] S. Abdelmounaime, H. Dong-Chen, "New Brodatz-based image databases for grayscale color and multiband texture analysis", *ISRN Machine Vision*, vol. 2013, 876386, 2013. doi:10.1155/2013/876386.

[24] T. Randen, J.H. Husoy, "Filtering for Texture Classification: A comparative study", *IEEE Trans Pattern Analysis and Machine Intelligence*, vol. 21, pp. 291-310, 1999.

[25] R. Picard, T. Kabir, F. Liu, "Real-time recognition with the entire Brodatz texture database," *Proc. Computer Vision and Pattern Recognition*, pp. 638-639, 1993.

[26] X. Liu, D. Wang, "Texture classification using spectral histograms", *IEEE Trans Image Processing*, vol. 12, pp. 661-670, 2003.